Multiphoton-detachment cross sections for H^-

Sydney Geltman
Joint Institute for Laboratory Astrophysics, University of Colorado and National Institute of Standards and Technology, Boulder, Colorado 80309-0440
(Received 17 December 1990)

Perturbation theory is applied to the evaluation of the multiphoton-detachment cross sections of H^- in a number of approximations. The zero-range plane-wave approximation is the simplest, as its effective dipole matrix element is reducible to a recursive differentiation, and it is applied to the one- to seven-photon-detachment processes. Improvements on this are made in the bound state by means of a short-range potential model and a dynamic screening representation, and in the continuum wave functions with the use of the best previously calculated e-H($1s$) singlet scattering phase shifts. The dynamic screening parameters are adjusted to give a good fit of the resulting one-photon cross section to its correct well-known value, and the accurate phase shifts effectively include all the important correlation effects in the free-free amplitudes. These improved wave functions are used for the evaluation of the two- and three-photon generalized detachment cross sections by explicitly carrying out all intermediate state sums. Our best $\hat{\sigma}_2$ and $\hat{\sigma}_3$ are estimated to be accurate to order 5%. The present theoretical results are compared with other calculations and recent measurements, revealing areas of agreement as well as certain discrepancies.

I. INTRODUCTION

The photodetachment of H^- has long been a process of great astrophysical interest because of its importance in the radiation equilibrium of the sun's photosphere. This motivated many calculations of its cross section with relatively simple wave functions, mainly by Chandrasekhar and his associates,[1] starting in the 1940s. Laboratory beam measurements[2] were carried out in the 1950s with flash lamps and filters between 4000 and 13 000 Å where this cross section has its largest values. The then increasing availability of large-scale computers led to accurate Hylleraas-type calculations[3] on the bound state of H^- as well as to variational and close-coupling treatments of the e-H($1s$) low-energy elastic scattering.[4] These latter continuum wave functions represent the final states in the photodetachment process, and led to further improvements in the calculated photodetachment cross section.[5–8]

There was close mutual agreement among the various calculations using these highly correlated bound and continuum functions. These were also in excellent agreement with the measured cross section,[2] and so it was felt that the one-photon-photodetachment cross section for H^- was finally accurately known.

As lasers came into use and the study of intense field nonlinear processes became feasible, the multiphoton detachment of negative ions became a subject of experimental and theoretical interest.[9,10] The H^- ion is the simplest negative ion, and thus is the prototype system in which one might expect the most detailed understanding of these processes. A number of subsequent theoretical calculations[11–13] on the two-photon detachment of H^- gave rather divergent results for this process, unlike the close agreement[5–7] obtained in the one-photon case. On the experimental side, the absence of high-power laser sources at variable photon energies below the binding energy of 0.754 eV held back progress on normal cross-beam studies.

This unavailability of suitable high-power laser sources was overcome recently by Tang *et al.*[14] with the use of relativistic H^- beams at the Los Alamos Meson Physics Facility. By intersecting this fast ion beam with a beam of CO_2 laser pulses at varying angles, they were able to obtain Dopper-shifted photon energies (0.117 eV in the laboratory frame) according to $h\nu=[(1+\beta\cos\alpha)/(1-\beta^2)^{1/2}]h\nu_0$, which vary between 0.08 and 0.43 eV in the atom frame. This corresponds to two- to nine-photon multiphoton detachment (MPD) processes. With the continuing improvement of these measurements we can expect a wealth of new data on MPD cross sections for H^-, and this is the motivation for the present theoretical work.

In this paper we will begin in Sec. II with the background theory for the formulas for n-photon detachment as derived from perturbation theory for applied radiation fields which are sufficiently weak. We will then review in Sec. III the previous work in arriving at the now well-established result for the one-photon detachment. Going on to multiphoton calculations in Sec. IV, we will introduce the simplest approximation, the zero-range plane-wave (ZRPW) approximation. Improved calculations on two- and three-photon detachment will be covered in Sec. V. Finally, our results will be compared with the latest experimental data available and with other calculations in Sec. VI, and the conclusions summarized in Sec. VII.

II. BACKGROUND THEORY FOR MPD CROSS SECTIONS

Let us consider an atomic system initially in some bound state which is perturbed by a rectangular pulse of

duration τ and electric field $\mathbf{E}\cos\omega t$. The dynamical evolution of this system is governed by the time-dependent Schrödinger equation. Rather than writing this in its well-known partial differential equation form, it is more useful to write it in the form of the equivalent integral equation,

$$\Psi(\mathbf{r},t)=\Phi_b(\mathbf{r})e^{-i\varepsilon_b t} -i\int_0^t dt'\int d\mathbf{r}'G(\mathbf{r},t;\mathbf{r}',t')(\mathbf{E}\cdot\mathbf{r}') \times\cos(\omega t')\Psi(\mathbf{r}',t') . \quad (1)$$

(We use atomic units, $e=m=\hbar=1$, unless otherwise specified.) G is the kernel or Green's function for the free atom (states Φ_j, energies ε_j)

$$G(\mathbf{r},t;\mathbf{r}'t')=\sum_j \Phi_j^*(\mathbf{r})\Phi_j(\mathbf{r}')e^{-i\varepsilon_j(t-t')} . \quad (2)$$

In the weak-field case, where $E\ll 1$ atomic unit of electric field strength, we may solve (1) by iterating it n times. The projection of any final atomic state $\Phi_f(\mathbf{r})$ upon the thus iterated approximate solution $\Psi^{(n)}(\mathbf{r},\tau)$ leads to the atomic transition probability in the long τ limit (i.e., many cycles of the field)

$$p_f^{(n)}=\left[\frac{E}{2}\right]^{2n}2\pi\tau\delta(\varepsilon_f-\varepsilon_i-n\omega)|D_n|^2 , \quad (3)$$

where the effective dipole matrix element in lowest order is

$$D_n=\sum_{v_1,v_2,\ldots,v_{n-1}}\frac{\langle\Phi_b|d|\Phi_{v_1}\rangle\langle\Phi_{v_1}|d|\Phi_{v_2}\rangle\cdots\langle\Phi_{v_{n-2}}|d|\Phi_{v_{n-1}}\rangle\langle\Phi_{v_{n-1}}|d|\Phi_f\rangle}{(\varepsilon_i-\varepsilon_1+\omega)(\varepsilon_i-\varepsilon_2+2\omega)\cdots[\varepsilon_i-\varepsilon_{n-1}+(n-1)\omega]} \quad (4)$$

and d is the effective field-atom interaction operator. The factor $E/2$ arises from the rotating-wave approximation. The counterrotating part of $\cos\omega t$ is negligible since it is of higher order, or will correspond to the absorption of more than n photons. All of the many-electron wave functions Φ_j are taken to be normalized to unity in a large quantization volume for the configuration space of each of the electrons. The effect of this condition is to require the wave function of the ejected electron to go to unit amplitude asymptotically.

The total transition probability requires a sum over all possible final states, which, if we are dealing with a single-electron detachment process into a final state continuum, gives

$$P_n=(2\pi)^{-3}\int d\mathbf{k}_f p_f^{(n)} =(2\pi)^{-2}(E/2)^{2n}\tau k_f\int d\hat{\mathbf{k}}_f|D_n|^2 . \quad (5)$$

This is the general Fermi golden rule for an n-photon bound-free transition probability, where k_f is now the ejected-electron wave number as fixed by energy conservation, $k_f^2/2=n\omega+\varepsilon_b$ and ε_b is the bound state. This leads to the definition of a generalized cross section $\hat{\sigma}_n$, in terms of which the total probability is expressed in the form

$$P_n=\hat{\sigma}_n F^n\tau , \quad (6)$$

where F is the incident photon flux. Note from this definition that the cgs dimensions of the generalized cross section are $\mathrm{cm}^{2n}\,\mathrm{s}^{n-1}$.

In terms of the energy flux I (laser intensity)

$$F=\frac{I}{\omega}=\frac{E^2}{8\pi\alpha\omega} , \quad (7)$$

where $1/\alpha$ equals the velocity of light in atomic units. Combining (5), (6), and (7) gives us the formula for the generalized MPD cross section

$$\hat{\sigma}_n=(2\pi)^{-2}(2\pi\alpha\omega)^n k_f\int d\hat{\mathbf{k}}_f|D_n|^2 . \quad (8)$$

The generalized MPD cross section is a purely atomic property, and the above derivation was carried out in terms of a rectangular perturbing pulse of radiation of duration τ. It is expected that a Gaussian pulse of full width at half maximum (FWHM) τ would lead to a final transition probability P_n which differs from (6) only by a small amount.

III. REVIEW OF WORK ON ONE-PHOTON DETACHMENT

A review of the theoretical work on the $\hat{\sigma}_1$ of H^- will be useful in assessing the approximations to be used for the higher-order $\hat{\sigma}_n$'s. One property of $\hat{\sigma}_1$ that does not apply to other $\hat{\sigma}_n$ is that it is independent of the polarization of the applied radiation. Thus the proper result for unpolarized radiation, which applies to most astrophysical applications, will follow from any calculation using a linearly or circularly polarized electric field.

The earlier calculations[1] of D_1 involved bound-state wave functions of the form of symmetrized (singlet state) products of purely radial functions in each of the electrons which were variationally found to minimize the energy. This evolved from the simple forms $\exp[-\beta(r_1+r_2)]$ and $\exp[-(\beta r_1+\gamma r_2)]+\exp[-(\beta r_2+\gamma r_1)]$ to forms of the Hylleraas type $\Phi_b(r_1,r_2,r_{12})$ where electron-electron correlation was explicitly included. The final state Φ_f was taken to be a symmetrized product of the residual $\psi_{1s}(r_1)$ and an ejected-electron wave, most simply taken as a plane wave, then a scattering wave function in the static field of the residual H(1s)

atom (Hartree approximation), and finally more sophisticated scattering treatments which also included correlation effects. Among these are scattering variational treatments of the Kohn or Hulthen form[5] and close-coupling calculations[6] (Hartree-Fock treatment of continuum states).

Our formulation of the theory in Sec. I is based on the so-called "length" form of the field-atom interaction $\mathbf{E}\cdot\mathbf{r}$. As is well known, the "length" matrix element is related to the "velocity" and "acceleration" forms by the transformations

$$\langle\Phi_i|z|\Phi_j\rangle=\left\langle\Phi_i\left|\frac{\partial}{\partial z}\right|\Phi_j\right\rangle\Big/(\varepsilon_i-\varepsilon_j)$$
$$=\left\langle\Phi_i\left|\frac{\partial}{\partial z}V\right|\Phi_j\right\rangle\Big/(\varepsilon_i-\varepsilon_j)^2 . \quad (9)$$

This identity holds when Φ_i and Φ_j are *exact* solutions for the free-atom Schrödinger equation $(T+V-\varepsilon_i)\Phi_i=0$. As all the H^- wave functions used in the evaluation of $\hat{\sigma}_1$ are approximate, since exact solutions for the two-electron problem do not exist, different values for $\hat{\sigma}_1$ will arise from each of the forms of the matrix element in (9). It is argued that the closeness of the three results, $\hat{\sigma}_1(L)$, $\hat{\sigma}_1(V)$, and $\hat{\sigma}_1(A)$, will be an indication of their overall correctness. Doughty, Fraser, and McEachran[6] have made a systematic study of the convergence of $\hat{\sigma}_1$ in its various forms as the bound and continuum (^1P state) wave functions are improved. While keeping the same continuum state (1*s*-2*s*-2*p* close-coupling approximation) they observed the change in $\hat{\sigma}_1(L)$ with a series of 3-, 6-, 11-, 20-, and 70-term bound-state functions, the largest of these being the bound state evaluated by Schwartz.[3] As the bound-free matrix element D_1 is dependent on the singlet *P*-wave phase shift, they have shown how these phase shifts change as the number of basis states is increased in the close-coupling expansion, up to 1*s*-2*s*-2*p*-3*s*-3*p*-3*d*. Finally, they show a series of $\hat{\sigma}_1(L),\hat{\sigma}_1(V),\hat{\sigma}_1(A)$ results corresponding to the Schwartz 70-parameter bound state and a series of continuum functions from 1*s* to 1*s*-2*s*-2*p*-3*s*-3*p*-3*d*. As expected, the spread between the three forms of $\hat{\sigma}_1$ decreased uniformly as the continuum function was improved, but rather than converging to a *single* curve, each form of $\hat{\sigma}_1$ converged to its own limit. In that limit $\hat{\sigma}_1(L)$ and $\hat{\sigma}_1(V)$ differed by $\sim 10\%$, and $\hat{\sigma}_1(V)$ and $\hat{\sigma}_1(A)$ differed by $\sim 20\%$. Since $\hat{\sigma}_1(V)$ uniquely agrees with the experiment to within the experimental error bars, and it is in $\sim 1\%$ agreement with other detailed theoretical calculations,[5,7,8] it is generally accepted that $\hat{\sigma}_1$ for H^- is known to $\lesssim 1\%$ accuracy. This accurate $\hat{\sigma}_1$ is shown in Fig. 1. The reason for the larger discrepancies between the accurate $\hat{\sigma}_1(V)$ and the less accurate $\sigma_1(L)$ and $\hat{\sigma}_1(A)$ is believed due to the velocity dipole operator's weighting of an intermediate region of $\mathbf{r}_1,\mathbf{r}_2$ space which is also the region contributing most to the binding energy, or where the variational bound-state wave function is most correct. The acceleration and length dipole operators, on the other hand, tend to weight the inner and outer spatial regions, respectively,

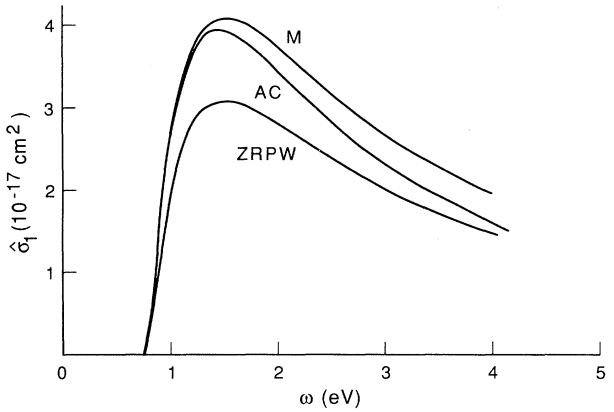

FIG. 1. Calculated $\hat{\sigma}_1$. Abbreviations: *M* (model potential), AC (accurate result based on fully correlated calculations), ZRPW (zero-range plane-wave).

where a smaller contribution is made to the bound-state energy, and hence there is less accuracy in those parts of the bound-state wave function.

An understanding of $\hat{\sigma}_1$ and its bound-free matrix element is important as a basis for going on to higher-order MPD processes. If we examine the effective matrix element (4) for an *n*-photon detachment, we see that it consists of a bound-free amplitude $\langle\Phi_b|d|\Phi_{v_1}\rangle$, followed by a series of mainly free-free amplitudes each representing a step in the total *n*-photon process. There may also be subsequent returns to the bound state as an intermediate state; for example, in the three photon process we may have the $b\rightarrow kp\rightarrow b\rightarrow k_fp$ sequence. Thus, in addition to accurately representing the bound-free amplitude as in $\hat{\sigma}_1$, we need to understand and get the best possible values for the subsequent free-free amplitudes. Although a number of free-free absorption calculations[15] have been done for electrons on hydrogen atoms, these results are generally given in averaged forms which are not useful for the amplitudes needed here. The important parameters for describing free-free amplitudes are the elastic scattering phase shifts, in this case for the singlet electron-atom system. They have been very accurately evaluated for $L=0$ and 1 using correlated functions in a scattering variational method by Schwartz[16] and Armstead.[17] For $L=2$, Gailitis[18] has obtained the best values by a close-coupling calculation, and for $l\geq 3$ an accurate representation at low energies is obtained from the effective range formula[19]

$$\tan\delta_l\cong\frac{\pi\alpha_H k^2}{8(l+\frac{3}{2})(l+\frac{1}{2})(l-\frac{1}{2})} , \quad (10)$$

where $\alpha_H=4.5$ a.u. is the polarizability of the ground-state H atom.

Unfortunately, the most accurate values of the bound-free *amplitudes* as functions of $\mathbf{k}_f$ which have been used for the best evaluations of $\hat{\sigma}_1$ are not available to us as a basis for calculating higher-order $\hat{\sigma}_n$. It will therefore be necessary to make use of a simpler model system for H^-,

which we will parametrize to give the correct $\hat{\sigma}_1$, and thus hopefully a good bound-free amplitude as a springboard for the higher $\hat{\sigma}_n$. We take a model that we have used many years ago,[20] based on the short-range cutoff Coulomb potential

$$V=\begin{cases}-\frac{1}{r}+\frac{1}{r_0}, & r<r_0\\ 0, & r\geq r_0\ .\end{cases} \tag{11}$$

Taking r_0 such that this potential will accommodate only one bound s state at the known binding energy of H^-, 0.754 eV, gives $r_0=1.88$ a.u. If $\phi_0(r)$ is thus the bound state and $\phi_{\mathbf{k}}(r)$ are the corresponding continuum functions in this potential, then the model two-electron singlet wave functions

$$\Phi_b=\phi_0(r_1)\phi_0(r_2)\ , \tag{12}$$

$$\Phi_{\mathbf{k}}=\frac{1}{\sqrt{2}}[\phi_0(r_1)\phi_{\mathbf{k}}(\mathbf{r}_2)+\phi_0(r_2)\phi_{\mathbf{k}}(\mathbf{r}_1)] \tag{13}$$

may be used to evaluate a model $\hat{\sigma}_1$ following the formulas in Sec. II. This resulting $\hat{\sigma}_1$ (model) is shown in Fig. 1. It agrees closely with $\hat{\sigma}_1$ (accurate) just above threshold but becomes too large by about 20% at higher photon energies.

Our simple model has used a continuum wave function $\Phi_{\mathbf{k}}$ which does *not* satisfy the correct boundary condition,

$$\Phi_{\mathbf{k}}\underset{r_2\to\infty}{\sim}\frac{1}{\sqrt{2}}\psi_{1s}(r_1)F_{\mathbf{k}}(\mathbf{r}_2)\ , \tag{14}$$

where ψ_{1s} is the hydrogen ground state and $F_{\mathbf{k}}$ is the correct scattering wave of asymptotic unit amplitude. Using ψ_{1s} instead of ϕ_0 in (13) would have the effect of decreasing $\hat{\sigma}_1$ (model) by the square of the overlap integral $\Delta=\int d\mathbf{r}\,\phi_0\psi_{1s}=0.911$, which would bring $\hat{\sigma}_1$ (model) and $\hat{\sigma}_1$ (accurate) into better agreement at higher energies but reduce the agreement near threshold. The best overall agreement is obtainable by representing the residual bound electron as an energy-dependent mixture of $\phi_0(r)$ and $\psi_{1s}(r)$, which we may interpret as a dynamic screening effect. When the ejected electron is very slow it will provide enough effective screening so that the screened function ϕ_0 is a reasonable choice, and when it is fast one would expect minimal screening, or ψ_{1s} as the best representation for the residually bound electron. We parametrize the bound orbital as

$$\xi(r;k)=[1-f(k)]\phi_0(r)+f(k)\psi_{1s}(r)\ , \tag{15}$$

with $f(k)=1-\exp(-ak^n)$, and carry out a least-squares fit of $\hat{\sigma}_1$ (model) to $\hat{\sigma}_1$ (accurate) by varying the dynamic screening parameters a and n. This leads to a fit of the cross sections to within $\leq 2\%$ over the entire energy range of Fig. 1, with best-fit parameters $a=46.25$ and $n=3.0$. This improved model will now serve as the basis of evaluations of $\hat{\sigma}_2$ and $\hat{\sigma}_3$ in Sec. V of this paper.

IV. ZERO-RANGE PLANE-WAVE APPROXIMATION

Before proceeding on to the evaluation of improved MPD cross sections based on the very accurate calculations of $\hat{\sigma}_1$ and of e-H($1s$) elastic phase shifts, let us look at the following simplest description of the MPD process. Consider the one-electron process originating in the zero-range bound state

$$|b\rangle=\left[\frac{b}{2\pi}\right]^{1/2}e^{-br}/r\ , \tag{16}$$

and involving intermediate and final states which are simply plane waves. The bound-free dipole matrix element in the "length" form and linearly polarized radiation is

$$D_1=\langle b|z|\mathbf{k}\rangle=8i\left[\frac{\pi b}{2}\right]^{1/2}\frac{k_z}{(b^2+k^2)^2}\ . \tag{17}$$

Propagating this through the various continuum intermediate states in (4), the effective free-free amplitudes are

$$\langle\mathbf{k}|z|\mathbf{k}'\rangle=\int d\mathbf{r}\,ze^{i(\mathbf{k}'-\mathbf{k})\cdot\mathbf{r}}$$
$$=-i(2\pi)^3\frac{\partial}{\partial k_z}\delta(\mathbf{k}-\mathbf{k}')\ . \tag{18}$$

This simple form allows us to trivially carry out successive integrals over continuum intermediate states by means of partial integrations, giving the recurrence relation for the effective nth-order dipole matrix element

$$D_n=-2\frac{\partial}{\partial k_z}\frac{D_{n-1}}{k^2+b^2-2(n-1)\omega}\ . \tag{19}$$

This method works equally well for the case of circularly polarized radiation where the dipole operator is $\frac{1}{2}(x\pm iy)$. The simplicity of this recurrence relation allows for the rapid evaluation of D_n for arbitrary n. As a practical matter, the algebraic expressions arising from the successive differentiations become quite cumbersome and numerical differentiation is useful, as well as a numerical integral over final ejection angle. The resulting one-electron cross section should be multiplied by 2 to account for both equivalent electrons in H^-. We have applied this zero-range plane-wave approximation to H^- for $n\leq 7$.[21] The result for $\hat{\sigma}_1$ is shown in Fig. 1, and is seen to lie $\sim 20\%$ below the accurate curve in the energy range just above threshold, where the model result is much closer to the accurate curve. Since the model ϕ_0 has the same form as the zero-range $|b\rangle$, this 20% difference is mainly the result of the difference in normalization constants. The zero-range normalization constant is about 15% below the model one because the zero-range function gets much larger than the model one for $r<r_0$, a region which gives a negligible contribution to the length dipole matrix element. At larger photon energies the difference in shapes of the model and ZRPW curves for $\hat{\sigma}_1$ arises from the non-negligible contribution of the model p-wave phase shifts in the final state.

The ZRPW results for $\hat{\sigma}_n$ for linear polarization and $7\geq n\geq 2$ have been previously given[21] over the photon energy region between threshold energy, $|\varepsilon_b|/n$, and the

next higher threshold, $|\varepsilon_b|/(n-1)$. As the next higher threshold is crossed and $(n-1)$-photon detachment becomes the lowest-order MPD process, the n-photon detachment still remains as an "above-threshold detachment" (ATD) peak (in terms of the ejected-electron energy distribution) in analogy with above-threshold ionization (ATI) peaks in ionization. When a new threshold is crossed in this way the last factor in the energy denominator in (4) is such that $\varepsilon_b-\varepsilon_{n-1}+(n-1)\omega$ goes through a zero in the integration range $0\le\varepsilon_{n-1}<\infty$. While this pole may complicate the intermediate-state sum in a precise calculation, it is harmless in the ZRPW approximation because of the effective $\delta(\varepsilon_{n-1}-\varepsilon_f)$ and the pole's never coinciding with ε_f. This leads to $\hat{\sigma}_n$ and their derivatives being continuous across new thresholds in the ZRPW approximation.

The Wigner law for the threshold shape is governed by the lowest orbital angular momentum quantum number l_0 in the final state, i.e., $\sigma\sim k_f^{2l_0+1}$. Since $l_0=1,0,1,0,\ldots$ for $n=1\text{-},2\text{-},3\text{-},4\text{-},\ldots$ photon-detachment for the linear polarization case, σ_n will alternate between the threshold forms $(\omega-\varepsilon_n)^{3/2}$ and $(\omega-\varepsilon_n)^{1/2}$. In circular polarization the selection rule $\Delta l=1$ leads to $l_0=n$ for n-photon detachment, and the threshold forms $(\omega-\varepsilon_n)^{n+1/2}$. The threshold behaviors for the linear polarization case would show up as a series of discontinuities in the total detachment probability over an extended frequency range, as is seen in the Tang *et al.*[14] measurements. On the other hand, these discontinuities would not be expected with circularly polarized radiation because of the always vanishing derivatives at thresholds.

The occurrence of a new channel for MPD with the infinite slope threshold form $\hat{\sigma}_n\sim(\omega-\varepsilon_n)^{1/2}$ must be accompanied by a cusp in the old channels $\hat{\sigma}_{n+1}$ in order that total absorbed photon flux vary smoothly across these thresholds. This is the analog of the Wigner cusp in electron-atom scattering when a new excitation channel opens up. We saw above that this feature is missed in the ZRPW approximation because there new poles do not affect the intermediate-state integrals.

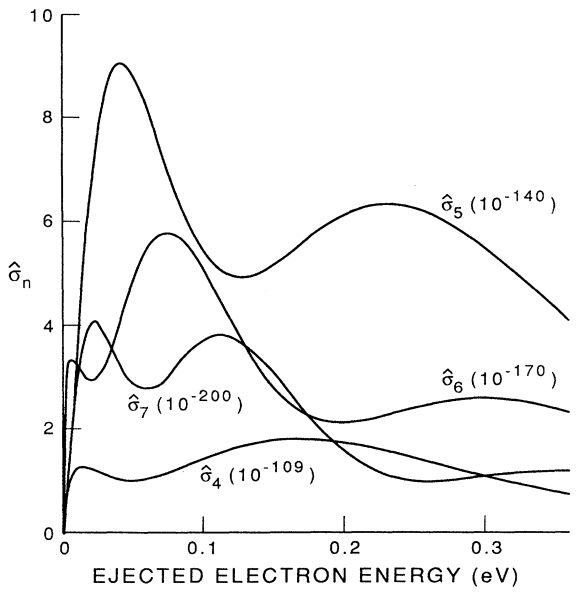

FIG. 2. Generalized cross sections in the ZRPW approximation for linear polarization. Each $\hat{\sigma}_n$ is in units of $\mathrm{cm}^{2n}\mathrm{s}^{n-1}$ and has the power of 10 indicated in parentheses.

In Fig. 2 we show the ZRPW results for $\hat{\sigma}_n$ in linear polarization over an extended range of ejected-electron energies which cover the crossing of several higher thresholds. We have seen in Ref. 21 a detailed comparison of this $\hat{\sigma}_2$ with other calculations from the literature. The wide spread in these values was quite surprising, and indicated the large degree of theoretical uncertainty in $\hat{\sigma}_2$, as opposed to the present universal agreement of many calculations on $\hat{\sigma}_1$. This provided motivation for the more precise calculations of $\hat{\sigma}_2$ which we present in the following sections. Another motivation is to try to assess the accuracy of the ZRPW approximation since it can so easily be applied to much higher values of n.

In Ref. 21, we also compared our ZRPW results with the early results of Tang *et al.*[14] We found a qualitative agreement in relative magnitudes over the $n=3$–7 photon range. In comparing our $\hat{\sigma}_3$ with a later measurement of Smith *et al.*[22] over the $n=3$ region there appeared some significant differences near threshold, and this provided additional motivation for a better calculation of $\hat{\sigma}_3$, which is also done in the following sections.

V. IMPROVED CALCULATIONS FOR $\hat{\sigma}_2$ AND $\hat{\sigma}_3$

In seeking to go beyond the ZRPW approximation we will apply two improved methods. They both are based on the approximate H^- wave functions for the bound-free amplitude,

$$\Phi_b=\phi_0(r_1)\phi_0(r_2)\,, \tag{20}$$

$$\Phi_{\mathbf{k}}=\frac{1}{\sqrt{2}}[\xi(r_1;k)\phi_{\mathbf{k}}(\mathbf{r}_2)+\xi(r_2;k)\phi_{\mathbf{k}}(\mathbf{r}_1)]\,, \tag{21}$$

where $\phi_0(r)$ is the initial model bound-state wave function[20] and ξ is the dynamically screened residual bound-state function defined in (15). As we have seen in Sec. III these wave functions lead to a $\hat{\sigma}_1$ which is generally within 2% of the most accurate correlated calculation of $\hat{\sigma}_1$.

This should provide us with accurate values of the $\langle\Phi_b|d|\Phi_{v_1}\rangle$ bound-free matrix elements in (4) as the first step in the nth-order process. It must be noted that the least-squares fitting of $\hat{\sigma}_1$ with parameters in ξ only guarantees a good value for $|\langle\Phi_b|d|\Phi_{v_1}\rangle|^2$, but there is no reason to expect an incorrect phase while getting a correct amplitude in this fitting procedure. The fitting was based on the reasonable physical assumption of dynamic screening by the ejected electron.

The first of our improved methods for higher-order $\hat{\sigma}_n$ is called "model," and it will use the $\phi_{\mathbf{k}}$ corresponding to our model cutoff Coulomb potential in the evaluation of subsequent free-free amplitudes.

The second method will use continuum wave functions

which contain the best phase shifts available for e-H($1s$) singlet scattering[16–18] as discussed in Sec. III. These latter calculations are the result of highly correlated trial functions for Φ_k in which the asymptotic forms become

$$\Phi_k \underset{r_2\to\infty}{\sim} \frac{1}{\sqrt{2}}\psi_{1s}(r_1)\sum_l i^l(2l+1)P_l(\hat{\mathbf{k}}\cdot\hat{\mathbf{r}})\frac{\chi_l(r_2)}{kr_2}\ , \tag{22}$$

with

$$\chi_l(r)\to kr[\cos\delta_l j_l(kr)-\sin\delta_l n_l(kr)]\ . \tag{23}$$

In this method, which we call the "best phase" approximation, we adopt asymptotoic form (23) for $\chi_l(>r_0)$. For $r<r_0$ we take χ_l as a continuous solution in the cutoff Coulomb potential. This will necessarily involve a discontinuity in χ_l' at r_0, which has no appreciable effect on the magnitude of the length form of the free-free radial matrix elements. Although many correlation terms are needed in an accurate variational or close-coupling calculation for the scattering phase shifts, these terms come into play in the finite volume where electron-electron interactions are important. The correlations do not persist explicitly into the singly asymptotic region of Eq. (22), but of course, their effects are contained in the asymptotic phase shifts. This is similar to the effects of a nonlocal, short-range optical potential in giving rise to characteristic asymptotic phase shifts. The dipole matrix element in its length form will give greatest weight to the outermost parts of the wave functions, where we expect them to be essentially exact with the correct phase shifts. Thus we expect a very good description of all the free-free amplitudes in (4) in this "best phases" approximation. The "model" and "best" phase shifts are given in Fig. 3.

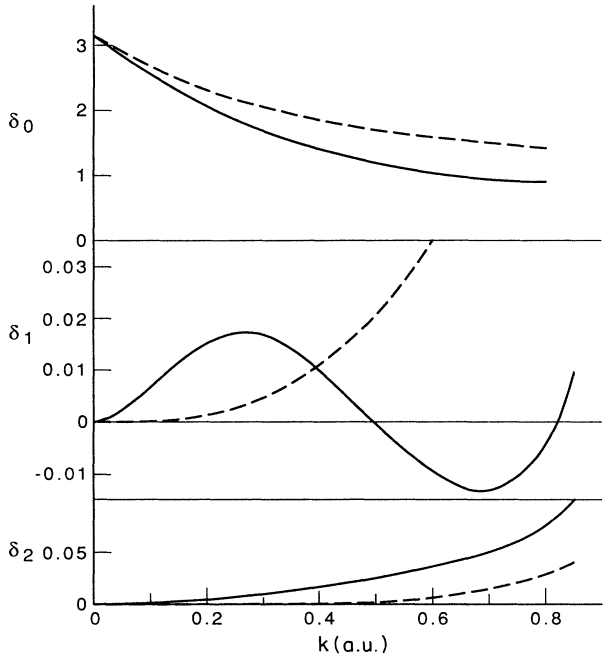

FIG. 3. Electron-H($1s$)^1S, ^1P, and ^1D elastic scattering phase shifts δ_l (in radians): Best phase (solid lines) and model phase (dashed lines).

Below we write down the resulting explicit expressions for $\hat{\sigma}_2$ and $\hat{\sigma}_3$ in linear polarization,

$$\hat{\sigma}_2=\frac{8\pi}{9k_f}(8\omega\alpha)^2\left[\left|\int_0^\infty dk\frac{M_{b1}(k)M_{10}(k,k_f)}{\varepsilon_b-\varepsilon_k+\omega}\right|^2+\frac{4}{5}\left|\int_0^\infty dk\frac{M_{b1}(k)M_{12}(k,k_f)}{\varepsilon_b-\varepsilon_k+\omega}\right|^2\right], \tag{24}$$

$$\begin{aligned}\hat{\sigma}_3=\frac{8}{k_f}(8\omega\alpha)^3\Bigg[\frac{1}{27}\Bigg|&\int_0^\infty dk'\frac{M_{01}(k',k_f)}{\varepsilon_b-\varepsilon_{k'}+2\omega}\int_0^\infty dk\frac{M_{b1}(k)M_{10}(k,k')}{\varepsilon_b-\varepsilon_k+\omega}\\&+\frac{4}{5}\int_0^\infty dk'\frac{M_{21}(k',k_f)}{\varepsilon_b-\varepsilon_{k'}+2\omega}\int_0^\infty dk\frac{M_{b1}(k)M_{12}(k,k')}{\varepsilon_b-\varepsilon_k+\omega}+4\pi^2\frac{M_{b1}(k_f)}{2\omega}\int_0^\infty dk\frac{M_{b1}^2(k)}{\varepsilon_b-\varepsilon_k+\omega}\Bigg|^2\\&+\frac{4}{175}\left|\int_0^\infty dk'\frac{M_{23}(k',k_f)}{\varepsilon_b-\varepsilon_{k'}+2\omega}\int_0^\infty dk\frac{M_{b1}(k)M_{12}(k,k')}{\varepsilon_b-\varepsilon_k+\omega}\right|^2\Bigg]\ .\end{aligned} \tag{25}$$

Here $M_{b1}(k)$ is the bound-free radial integral

$$M_{b1}(k)=\eta(k)\int_0^\infty dr\, r^2\phi_0\chi_1\ , \tag{26}$$

where η is the dynamically screened overlap,

$$\eta(k)=\int d\mathbf{r}\,\phi_0(r)\xi(r;k) \tag{27}$$

and the free-free radial integral is

$$M_{ll'}(k,k')=\int_0^\infty dr\,\chi_l r\chi_{l'}\ . \tag{28}$$

Aside from phase-space constants and angular factors, these expressions represent the radial integrals involved in the respective paths from the initial bound state to the final free state. The two-photon cross section simply involves the two incoherent paths

$$b\to k,l=1\to\begin{cases}k_f,l_f=2\\k_f,l_f=0\ ,\end{cases}$$

while $\hat{\sigma}_3$ contains the three coherently interfering paths

$$b \rightarrow k, l=1 \rightarrow \begin{Bmatrix} k', l'=2 \\ k', l'=0 \\ b \end{Bmatrix} \rightarrow k_f, l_f=1 \ ,$$

as well as the incoherent one

$$b \rightarrow k, l=1 \rightarrow k', l'=2 \rightarrow k_f, l_f=3 \ .$$

The corresponding paths for circular polarization in $\hat{\sigma}_2$ and $\hat{\sigma}_3$ are those in which Δl and Δm equal 1 at each step. This results in the angular coefficients $\frac{4}{3}$ and $\frac{4}{175}$ in (24) and (25) being replaced by $\frac{2}{5}$ and $\frac{2}{35}$, respectively, to give $\hat{\sigma}_2$ and $\hat{\sigma}_3$ for circular polarization, after dropping the other nonparticipating channels.

All of the radial matrix elements are evaluated by numerical quadrature with the infinite limit taken as some large radius R. We have taken $R=100a_0,150a_0,200a_0$ and found that while each $M_{ll'}(k,k')$ changed with the choice of R, the subsequent integral over k remained converged, independent of R as long as R was large enough so that short-range contributions ($r<r_0$) become negligible. The integrand in k of an expression involving a factor $M_{ll'}(k,k')$ has oscillations which peak at $k=k'$, but are not as extremely localized as the $(d/dk)\delta(k-k')$ form which appears in the ZRPW approximation.

The effect of using dynamically screened ξ's in the free-free matrix elements rather than ϕ_0 or ψ_{1s} alone would be small, since $\int dr\, \xi(r;k)\xi(r;k')=1$ at $k=k'$, in which vicinity most of the free-free amplitude is concentrated, and that overlap cannot get below $\Delta=\int d\mathbf{r}\, \phi_0\psi_{1s}=0.911$. In fact, we have omitted the dynamic screening factors entirely in the evaluation of free-free matrix elements since the entire contribution comes from the asymptotic part of the free-electron wave functions, and the bound electron provides no further explicit dynamic role. Also, the contribution of the intermediate-state path which returns to the bound intermediate state in $\hat{\sigma}_3$ is found to be very small—less than 1% at all photon energies.

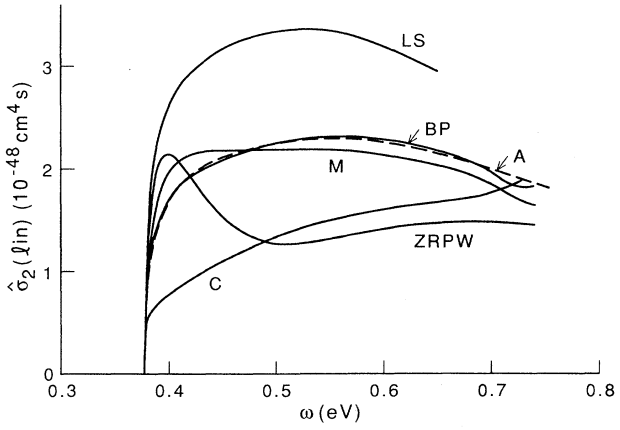

FIG. 4. Calculated $\hat{\sigma}_2$ for linear polarization. Abbreviations: *A* (Adelman, corrected, Refs. 11 and 23), BP and *M* (best phase and model, presently calculated), *C* (Crance, Ref. 25), LS (Liu and Starace, Ref. 27), ZRPW (Ref. 21 and presently calculated).

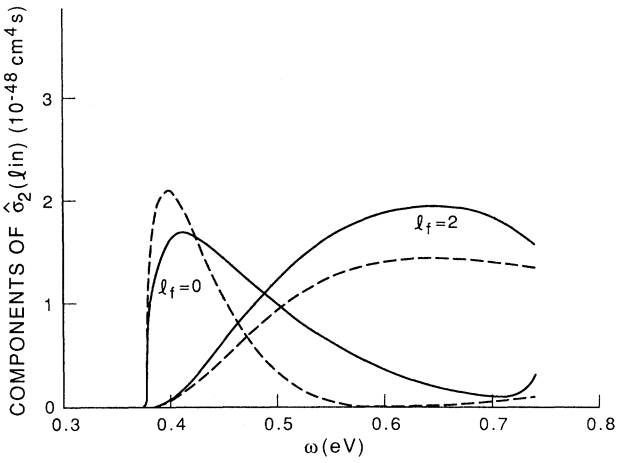

FIG. 5. Final *s*- and *d*-wave components of calculated $\hat{\sigma}_2$ for linear polarization: best phase (solid) and ZRPW (dashed).

The results for $\hat{\sigma}_2$ in linear polarization are given in Fig. 4. The closeness of our best phase result to $\frac{1}{2}$ of the Adelman[11] result is quite remarkable. That original result was indeed too high by a factor of 2 because the $1/\sqrt{2}$ normalization factor in $\Phi_{\mathbf{k}_f}$ was omitted.[23]

Adelman used an implicit technique to sum over intermediate states, but also used the accurate Schwartz phase shifts[16] for $l_f=0$. As the $l'=1$ and $l_f=2$ phase shifts are small, his neglect of them was reasonable. The difference between our best phase and model results is an indication of the error in the use of the model phase shifts (given in Fig. 3). The very different shape for $\hat{\sigma}_2$ in ZRPW is a result of the large error in using a plane-wave *s* wave in the

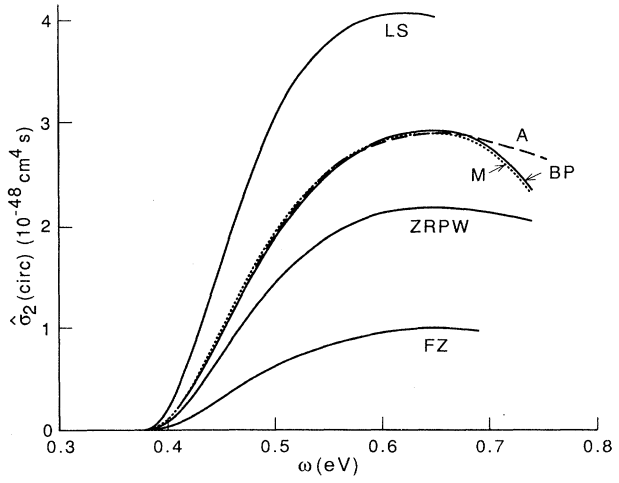

FIG. 6. Calculated $\hat{\sigma}_2$ for circular polarization. Abbreviations: *A* (Adelman, corrected, Refs. 11 and 23), BP and *M* (best phase and model, presently calculated), FZ (Fink and Zoller, Ref. 26), LS (Liu and Starace, Ref. 27), and ZRPW (presently calculated).

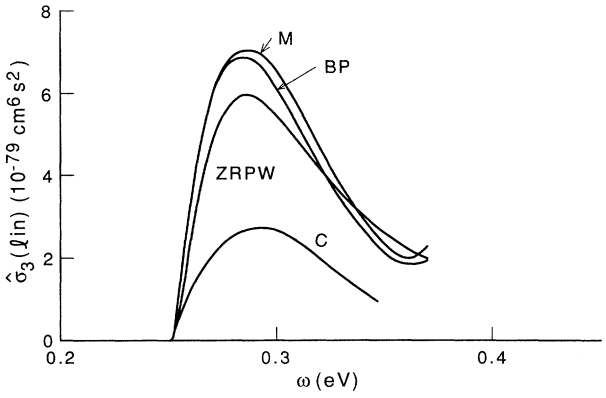

FIG. 7. Calculated $\hat{\sigma}_3$ for linear polarization. Abbreviations: *C* (Crance, Ref. 25), BP and *M* (best phase and model, presently calculated), ZRPW (Ref. 21 and presently calculated).

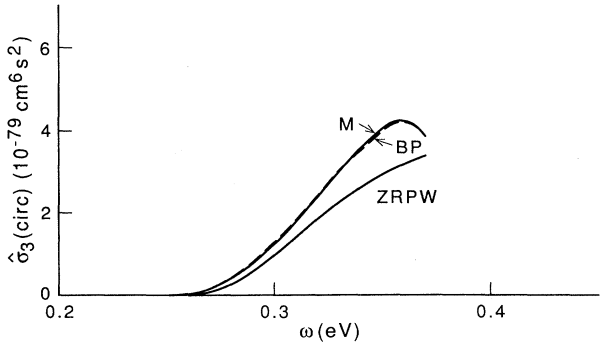

FIG. 9. Calculated $\hat{\sigma}_3$ for circular polarization. Abbreviations: BP and *M* (best phase and model), ZRPW (zero-range plane-wave), all presently calculated.

final state. One sees that this can lead to an appreciable error since the true *s*-wave phases start at π (because of the presence of one bound *s* state) and have appreciable values in the important range of k. This effect is more clearly displayed in Fig. 5 where $\hat{\sigma}_2$ for linear polarization is broken into its two final angular momentum components, $l_f=0$ and 2. Here it is seen that it is the difference in shape of the ZRPW $l_f=0$ component which is responsible for the difference in shape of the total $\hat{\sigma}_2$ seen in Fig. 4. The differences in magnitudes for the $l_f=2$ contributions are largely understood to arise from the low bound-state normalization factor in ZRPW, as discussed earlier. The results for $\hat{\sigma}_2$ in circular polarization are given in Fig. 6, and again we have the extreme closeness of the model, best phase, and corrected Adelman results, showing the relative unimportance of the small *p*- and *d*-wave phase shifts.

The three-photon results for linear polarization are shown in Fig. 7, the breakdown into $l_f=1$ and 3 components is given in Fig. 8, and the cross sections for circular polarization are given in Fig. 9. The closeness of the model and best phase results is an indication of the lesser effect of the small *p*- and *d*-wave phase shifts than is the case for the large *s*-wave phase shifts. The ZRPW result in linear polarization is relatively better for $\hat{\sigma}_3$ than for $\hat{\sigma}_2$, indicating the lesser relative importance of the *s*-wave continuum function to the total cross section.

One would expect this declining relative influence of the *s*-wave continuum function to continue into the ZRPW results for higher $\hat{\sigma}_n$ in linear polarization. In the high-n limit, the main error in the ZRPW approximation should be only the bound-state normalization, which can be corrected with the factor 1.3, as discussed earlier. It is a rather remarkable outcome that an approximation as simple as ZRPW can give the high-order MPD cross sections to such accuracy. The computation times on the VAX 8600 and 6400 are about 5 min for a set of $\hat{\sigma}_2$'s, and about 5 h for a set of $\hat{\sigma}_3$'s. This rapid escalation of machine time needed to do successive intermediate-state integrals is what prevents us from going to higher $\hat{\sigma}_n$ with the improved calculations. Perhaps the use of implicit summation techniques, such as used by Adelman,[11] might involve only a linear growth of machine time, and thus be feasible for higher orders.

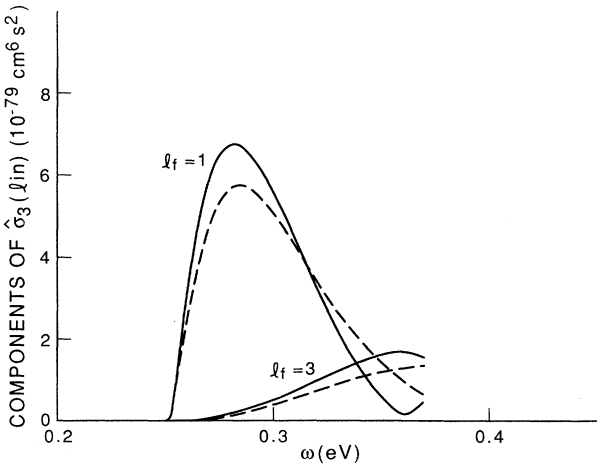

FIG. 8. Final *p*- and *f*-wave components of calculated $\hat{\sigma}_3$ for linear polarization: best phase (solid) and ZRPW (dashed).

VI. COMPARISONS WITH EXPERIMENT AND OTHER CALCULATIONS

The first MPD measurements by Tang *et al.*,[14] using Doppler tuning with obliquely crossed relativistic H^- and CO_2 laser beams, covered the photon energy range 0.10–0.32 eV in the atom's frame. The intensity in the laser pulse (I_0 in the laboratory frame) is transformed into an atom-frame intensity by

$$I=I_0(\omega/\omega_0)^2 . \tag{29}$$

We have in Ref. 21 evaluated the total MPD probability over this range using the ZRPW cross sections of Figs. 2 and 7 for $\hat{\sigma}_n$ ($n=3$–7), the transformed intensity of (29), the n-photon probability P_n formula of (6), and have

made allowance for initial-state depletion with

$$P=1-\exp\left[-\sum_n P_n\right] . \tag{30}$$

This sum starts at the minimum number of photons needed for detachment at ω, and goes over all higher ATD contributions. Using the estimated laboratory peak intensity of 2×10^{10} W/cm^2 in the above theoretical procedure resulted in essentially total detachment $P\cong1$ for all $\omega\gtrsim0.15$ eV ($n\geq5$), which correspond to much higher MPD probabilities than were observed. Only by using the reduced laboratory intensity of 1×10^{10} W/cm^2 were we able to obtain a qualitative overall fit to the measurement. The calculated MPD probabilities also include the atom-frame time spent in the laser field at each of the Doppler-tuning angles ($\tau\sim1/\sin\alpha$).

An improved measurement by the same group (Smith *et al.*[22]) concentrated on the three-photon region (0.25–0.37 eV). In Ref. 21, we also attempted to fit the measured detachment probability in this range with the ZRPW approximation for $\hat{\sigma}_3$, but it was found that to obtain a good fit one needed a $\hat{\sigma}_3$ in which (1) the maximum was shifted from 0.29 to 0.31 eV, (2) which rose from the threshold at 0.251 eV much more slowly than calculated, and (3) which decreased with energy beyond its maximum much more rapidly than calculated. It was felt that perhaps improved calculated values of $\hat{\sigma}_3$ would satisfy these requirements, but a glance at Fig. 7 shows that that is not the case, the model and best phase results being not appreciably different in shape from the ZRPW result.

More recent data obtained by this group of experimentalists[24] at the peak laboratory intensities 3.3, 6, and 12 GW/cm^2 over the photon energy range 0.24–0.39 eV continue to show the very slow rise from the three-photon threshold, which remains inconsistent with the presently calculated $\hat{\sigma}_3$. However, the very sharp dip at 0.38 eV found by Smith *et al.*[22] at 8 GW/cm^2 now appears to have diminished, in better agreement with the present $\hat{\sigma}_3$.

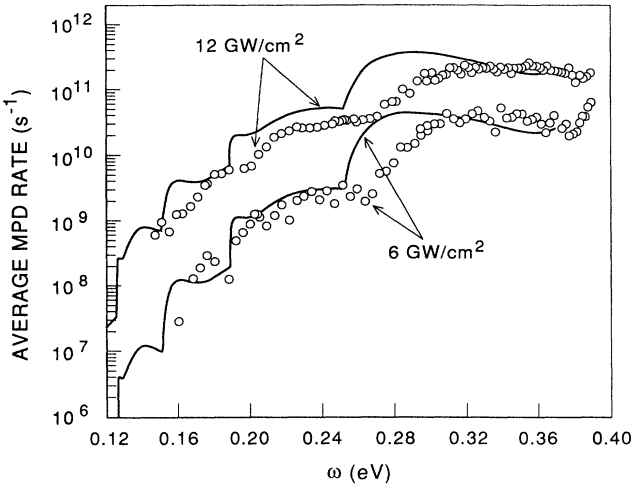

FIG. 10. Measured (Ref. 24) and presently calculated average multiphoton-detachment rates for Gaussian pulses with peak laboratory-frame intensities of 6 and 12 GW/cm^2.

In addition, new measurements[24] were obtained for the *absolute* mean detachment rate over the photon energy range 0.14–0.39 eV, covering three- to six-photon processes. We compare these measurements with our calculated rate for peak laboratory intensities of 6 and 12 GW/cm^2 in Fig. 10. The calculated rates are obtained by averaging present theoretical rates for a Gaussian pulse with maximum laboratory frame intensity

$$I_0(\rho)=I_{p0}e^{-\ln2(\rho/\rho_0)^2} , \tag{31}$$

which should apply to an H^- trajectory displaced by ρ from the axis of the laser beam with peak intensity I_{p0}, whose effective radius [half width at half maximum (HWHM)] is ρ_0. This leads to an average MPD rate

$$\bar{\Gamma}(\omega)=\frac{1}{2\ln2}\left[\frac{\pi}{\ln2}\right]^{1/2}(\rho_0/\rho_m)^2\sum_n \hat{\sigma}_n(\omega)F_p^n\Big/n\{1-\exp[-n\ln2(\rho_m/\rho_0)^2]\} , \tag{32}$$

where we are averaging over values of ρ lying between 0 and ρ_m, where atom frame $F_p=I_{p0}(\omega/\omega_0^2)$, and where again $n_{\min}$ in the sum is the minimum number of photons needed for detachment at ω. We use the ZRPW values for $\hat{\sigma}_4,\hat{\sigma}_5,\hat{\sigma}_6$, and the best phase value for $\hat{\sigma}_3$. Note that the average MPD rate decreases as ρ_m^{-2} and the choice of ρ_m is critical. We have taken $\rho_m=2\rho_0$ as the extent of the focal volume over which to evaluate the average calculated rates given in Fig. 10. With this choice of averaging, the agreement between measurement and theory is generally well within the estimated experimental uncertainty[24] of a factor of 5 as far as absolute values are concerned, but there remain serious discrepancies in the sharpness of the rises at several of the thresholds.

The data do not show the sharp onsets at the n-photon thresholds which are expected from the perturbation-theory calculation. This could be an indication that the nonperturbative aspects of the experimental conditions are significant. One such aspect is the shortness of the laser pulses in the atom frame. There are of the order of only ten laser cycles in the atom frame, which may be too short for the long-time limit taken in Sec. II to be valid. Another aspect is that the Keldysh adiabaticity parameter $\gamma=\omega b/E$ is of order 2, while it should be $\gg1$ for the

multiphoton-detachment-rate picture to be valid. This would imply that transient tunneling also plays a role in the detachment taking place in those measurements.

There have been a number of other recent theoretical calculations of these cross sections using various methods. We have already commented on the Adelman calculation[11,23] for $\hat{\sigma}_2$, as it is so very close to the present one in method and result. Crance[25] uses the dressed-atom (Floquet) picture to expand the entire time-dependent wave function in a finite basis of square integrable functions. The basis is taken to be large enough so that all important correlation effects are included. The ground state then appears as a resonance, whose width gives the detachment rate. Her results for $\hat{\sigma}_2$ and $\hat{\sigma}_3$ in linear polarization are also shown in Figs. 4 and 7, and they are seen to lie below our present results by about a factor of 2–3, although for $\hat{\sigma}_2$ they are closer at larger ω. We feel that the full correlation effects in the intermediate and final continuum states are taken into account in our best phase results, so we do not understand the reason for such a large difference with Crance's results. Fink and Zoller[26] have used an adiabatic hyperspherical approach to evaluate $\hat{\sigma}_2$ for the circular polarization case, and that result is included in Fig. 6. Liu and Starace[27] have also used an adiabatic hyperspherical-coordinate representation in a perturbative evaluation of $\hat{\sigma}_2$ and $\hat{\sigma}_3$, and their results, also shown in Figs. 4 and 7, appear to be about 50% higher than ours. Again the approach of these calculations is so different from ours that it is difficult to pinpoint the reason for the differences in results.

Mu and co-workers[28] use Keldysh-Faisal-Reiss methods to evaluate the H^- detachment rate, and have also found a satisfactory fit to the data of Tang *et al.*[14]

Becker, Long, and McIver[29] use as a potential model the three-dimensional regularized δ function, and find an integral form for the quasienergy in the Floquet picture. The imaginary part of the quasienergy is the desired detachment rate, which in the perturbative regime is related to the generalized MPD cross sections by $\Gamma=\sum_n \hat{\sigma}_n F^n$. This potential model is equivalent to a zero-range potential for the bound state, but it has a repulsive effect in the continuum, which differs from our taking plane waves in the ZRPW approximation. A comparison of the Becker, Long, and McIver result at their maximum Γ (and including a factor of 2 for the two initial equivalent bound electrons) for Γ/F^n for $n=2$ and 3 shows an effective maximum $\hat{\sigma}_2$ close to our best value, and an effective maximum $\hat{\sigma}_3$ about 0.5 of our best value.

Another study of Dörr *et al.*[30] evaluated detachment rates of H^- in a variety of approximations, including perturbation, Keldysh-Faisal-Reiss, and Floquet. Their results are roughly consistent with ours in the region where perturbation theory is expected to be valid.

A striking difference in the predictions of perturbation theory and the Floquet methods is the absence of threshold shifts in perturbation theory and the presence of pondermotive potential threshold shifts in the Floquet results. In fact, the addition of the invariant ponderomotive potential $E^2/4\omega^2$ to the atomic binding energy ε_b introduces the so-called "channel closings" each time $E^2/4\omega^2$ increases by one integer multiple of ω. The passage from n-photon to $(n+1)$-photon detachment by increasing the intensity at fixed frequency results in an abrupt decrease of detachment rate at these channel closings in Floquet calculations.

An alternative description is that the detachment *probability,* and not rate, is the fundamental physical quantity. That quantity for H^- is defined as

$$P(t)=1-|\langle\Phi_b(\mathbf{r})|\Psi(\mathbf{r},t)\rangle|^2 , \tag{33}$$

where Ψ is the full, exact time-dependent wave function as defined in (1) and Φ_b is the one bound-state stationary wave function. For weak enough fields where perturbation theory is valid, the approximate procedure we have used in our present calculation culminating in expressions (6) and (8) is satisfactory. However, it should be noted that rate behavior in perturbation theory, for example, expression (6), only results from a weak enough interaction and only in the long-time limit. In contrast, the rate Γ is an intrinsic quantity in a Floquet theory, arising as the imaginary part of the quasienergy.

If the field strength is too high the exact $P(t)$ will approach unity in a very unratelike manner. This departure of $P(t)$ from its perturbative ratelike behavior, which corresponds to n-photon absorption, may be called "tunneling" or "barrier suppression ionization (or detachment)," and total detachment may take place over times of the order of a period of the field or less. Such a regime is clearly not acceptable for a Floquet calculation in which the periodicity of the field is required to define the quasienergy, and where only after a large number of cycles of the field is that a meaningful entity. The onsets of tunneling or barrier suppression detachment are expected to be smooth, as a function of intensity. Thus, for a plot of P as a function of peak intensity for fixed frequency and pulse duration, one would expect a rising curve from $\hat{\sigma}_n F^n \tau$ at lowest intensity and converging to $P=1$ for large intensities (but not necessarily completely monotonic). We believe that these are fundamental questions that deserve additional theoretical study.

VII. CONCLUSIONS

We have evaluated the perturbative generalized cross sections for the multiphoton detachment of H^- in a variety of approximations. By far the simplest is the zero-range plane-wave approximation, in which a quick evaluation of high-order $\hat{\sigma}_n$'s is obtainable by recursive differentiation. The largest error in this procedure is the neglect of s-wave phase shifts in intermediate or final states, and shows up most markedly in $\hat{\sigma}_2$ for linear polarization. Apart from that case, all other $\hat{\sigma}_n$ in the ZRPW approximation appear to be quite good, after applying a correction factor of 1.3 arising from the low normalization constant in the bound state. Another convenient feature of the ZRPW approximation is that it is equally simple above new thresholds as it is in the minimum-photon region.

Two more precise approximations were applied to the evaluation of $\hat{\sigma}_2$ and $\hat{\sigma}_3$, which were based upon the elas-

tic e-H($1s$) singlet scattering phase shifts of a short-range potential model and upon the best calculated phases available. A dynamically screened $1s$ orbital for the residual electron was used to provide an accurate representation of the initial bound-free amplitude in the n-photon matrix element.

We thus expect our most accurate result to be that of the best phase approximation. It is difficult to assign an absolute percentage accuracy to this result, but we believe it to be of the order of 5% or better. One reason for this is that we are representing $\hat{\sigma}_1$ to $\leq 2\%$ accuracy with our choice of dynamical screening parameters in $\xi(r;k)$, and expect the bound-free amplitude to be equally accurate. Since highly accurate phase shifts are used for the remaining free-free amplitudes, we do not expect this accuracy to be appreciably degraded in the two- and three-photon processes. A second reason is that given by Adelman,[11] who felt that his $\hat{\sigma}_2$ should be good to 4.5% because similar calculations of the dynamic polarizability of H^- were that close to highly accurate variational results by Chung.[31] (The normalization correction of $\frac{1}{2}$ for Adelman's value of $\hat{\sigma}_2$ does not affect his result for the dynamic polarizability.) The extreme closeness of Adelman's corrected results to our best phase results for $\hat{\sigma}_2$ in linear and circular polarization (Figs. 4 and 6) lends additional support to our present error estimate.

While the overall agreement between theory and experiment in absolute detachment rate and its rough shape over the $n=3-6$ photon range is reasonable, there remain some troublesome discrepancies. In particular, the measured rises above the $n=3$- and 5-photon thresholds are much more slow and gradual than is indicated for the theory. We do not understand the reason for this behavior at this time.

It is hoped that additional tunable laser sources of sufficient power in the wavelength region of $\hat{\sigma}_2$ and $\hat{\sigma}_3$ may appear in the future to allow the measurement of these cross sections under more conventional laboratory conditions (i.e., thermal sources of H^-).

ACKNOWLEDGMENTS

I am indebted to S. A. Adelman, A. F. Starace, and C. Y. Tang for helpful discussions. Partial support was provided by National Science Foundation Grant No. PHY86-04504, and all computations were carried out on the JILA VAX 8600 and 6400.

[1]For a complete reference list see S. Chandrasekhar and D. D. Elbert, Astrophys. J. **128**, 633 (1958).
[2]L. M. Branscomb and S. J. Smith, Phys. Rev. **98**, 1028 (1955); S. J. Smith and D. S. Burch, *ibid.* **116**, 1125 (1959). A later absolute arc measurement was carried out by H. P. Popp and S. Kruse, J. Quant. Spectrosc. Radiat. Transfer **16**, 685 (1976).
[3]J. F. Hart and G. Herzberg, Phys. Rev. **106**, 79 (1457); C. L. Pekeris, *ibid.* **112**, 1649 (1958); C. Schwartz, *ibid.* **123**, 1700 (1961).
[4]P. G. Burke in, *Atomic Collision Processes,* edited by S. Geltman, K. T. Mahanthappa, and W. E. Brittin (Gordon and Breach, New York, 1968), pp. 1–55.
[5]S. Geltman, Astrophys. J. **136**, 935 (1962).
[6]N. A. Doughty, P. A. Fraser, and R. P. McEachran, Mon. Not. R. Astron. Soc. **132**, 2 (1966).
[7]J. T. Broad and W. P. Reinhardt, Phys. Rev. A **14**, 2159 1976.
[8]A. L. Stewart, J. Phys. B **11**, 3851 (1978).
[9]J. L. Hall, E. J. Robinson, and L. M. Branscomb, Phys. Rev. Lett. **14**, 1013 (1965).
[10]E. J. Robinson and S. Geltman, Phys. Rev. **153**, 4 (1967).
[11]S. A. Adelman, J. Phys. B **6**, 1986 (1973).
[12]M. Crance and M. Aymar, J. Phys. B **18**, 3529 (1985).
[13]G. P. Arrighini, C. Guidotti, and N. Durante, Phys. Rev. A **35**, 1528 (1987).
[14]C. Y. Tang, P. G. Harris, A. H. Mohagheghi, H. C. Bryant, C. R. Quick, J. B. Donahoe, R. A. Reeder, S. Cohen, W. W. Smith, and J. E. Stewart, Phys. Rev. A **39**, 6068 (1989).
[15]S. Geltman, Astrophys. J. **141**, 376 (1965); T. L. John, Mon. Not. R. Astron. Soc. **131**, 315 (1966); N. A. Doughty and P. A. Fraser, *ibid.* **132**, 267 (1966).
[16]C. Schwartz, Phys. Rev. **124**, 1468 (1961).
[17]R. L. Armstead, Phys. Rev. **171**, 91 (1968).
[18]M. Gailitis, in *Proceedings of the Fourth International Conference on the Physics of Electronic and Atomic Collisions, Quebec, 1965,* edited by L. Kerwin and W. Fite (Science Bookcrafters, Hastings-on-Hudson, 1965), p. 10.
[19]T. F. O'Malley, L. Spruch, and L. Rosenberg, J. Math. Phys. **2**, 421 (1961); B. R. Levy and J. B. Keller, *ibid.* **4**, 54 (1963).
[20]S. Geltman, Phys. Rev. **104**, 346 (1956).
[21]S. Geltman, Phys. Rev. A **42**, 6958 (1990).
[22]W. W. Smith, C. Y. Tang, C. R. Quick, H. C. Bryant, P. G. Harris, A. H. Mohagheghi, J. B. Donahue, R. A. Reeder, H. Sharifian, J. E. Stewart, H. Toutounchi, S. Cohen, T. C. Altman, and D. C. Rislove, J. Opt. Soc. Am. B **8**, 17 (1991).
[23]S. A. Adelman (private communication).
[24]C. Y. Tang, H. C. Bryant, P. G. Harris, A. H. Mohagheghi, R. A. Reeder, H. Sharifian, H. Toutounchi, C. R. Quick, J. B. Donahue, S. Cohen, W. W. Smith, and J. E. Stewart (unpublished).
[25]M. Crance, J. Phys. B **23**, L285 (1990).
[26]M. G. J. Fink and P. Zoller, J. Phys. B **18**, L373 (1985).
[27]C-R. Liu and A. F. Starace (private communication). The method used is similar to that used for $\hat{\sigma}_1$ in C.-H. Park, A. F. Starace, J. Tan, and C.-D. Lin, Phys. Rev. A **33**, 1000 (1986).
[28]X. Mu, Phys. Rev. A **42**, 2944 (1990); X. Mu, J. Ruscheinski, and B. Crasemann, *ibid.* **42**, 2949 (1990).
[29]W. Becker, S. Long, and J. K. McIver, Phys. Rev. A **42**, 4416 (1990).
[30]M. Dörr, R. M. Potvliege, D. Proulx, and R. Shakeshaft, Phys. Rev. A **42**, 4138 (1990).
[31]K. T. Chung, Phys. Rev. A **4**, 7 (1971).